Scientific Research Publishing

Advances in Nanoparticles, 2022, 11, 55-71
https://www.scirp.org/journal/anp
ISSN Online: 2169-0529
ISSN Print: 2169-0510

The Effects of an Inclined Magnetic Field, Brownian Motion, and Thermophoresis on the Flow of Electrically Conducting and Chemically Reacting Casson Nanofluids Using Soret-Dufour Mechanisms

Toyin Wasiu Akaje*, Bakai Ishola Olajuwon

Department of Mathematics, Federal University of Agriculture, Abeokuta, Nigeria
Email: *akajewasiu@gmail.com

How to cite this paper: Akaje, T.W. and Olajuwon, B.I. (2022) The Effects of an Inclined Magnetic Field, Brownian Motion, and Thermophoresis on the Flow of Electrically Conducting and Chemically Reacting Casson Nanofluids Using Soret-Dufour Mechanisms. *Advances in Nanoparticles*, **11**, 55-71.
https://doi.org/10.4236/anp.2022.112005

Received: February 21, 2022
Accepted: May 28, 2022
Published: May 31, 2022

Abstract

This research explored the effects of an angled magnetic field, Brownian motion, and thermophoresis on the flow of an electrically conducting and chemically reacting Casson nanofluid under the influence of the Soret-Dufour mechanism. A set of partial differential equations is generated by the flow mode. The governing partial differential equations are solved numerically using the spectral collocation method after being transformed to self-similar forms. The effect of various fluid parameters on the velocity profile, temperature profile, and nanoparticle concentration is addressed. A quantitative agreement is observed when previous findings are compared to the current results. The skin friction, local Nusselt number, and local Sherwood number are also examined, and the results are presented in the table. This study discovered that the inclined magnetic field has a significant impact on the flow of the electrically conducting fluid by delaying its mobility within the boundary layer. The plastic dynamic viscosity, which acts as a barrier to fluid flow, is shown to degenerate the fluid velocity when the Casson parameter is increased. As a consequence, the findings may be used to improve thermal science instruments and increase industrial output.

Keywords

Soret-Dufour Mechanism, Casson Nanofluid, Inclined Magnetic Field, Boundary Layer, Spectral Collocation Method

1. Introduction

The magnet of hydrodynamics (MHD) phenomenon describes the motion of electrically conducting fluids with a magnetic field. In recent years, several researchers have indicated an interest in researching comparable incidents. MHD research reveals application hall accelerators as well as MHD power producers. As a result of these applications, Alao *et al.* [1] (2016) investigated the impact of a magnetic field on the unsteady heat and mass transport of a reacting fluid as a result of these applications. Shahnaz *et al.* [2] (2021) have investigated the effect of an angled magnetic field and a decreasing sheet on Casson fluid motion. Saravana *et al.* [3] investigated the aligned magnetism effect on the fluid flow of Casson fluid across a non-uniform constant stretched surface (2019). Hashim *et al.* [4] (2020) discovered aligned magnetism in Williamson liquid during Newtonian heating of an elongating sheet. Furthermore, Yusuf and Mabood [5] (2020) examined the chemical reaction and aligned magnetic field effect in slippery Williamson liquid through a porous wall. Using the homotopy analysis technique, Jawad *et al.* [6] (2021) investigated 3-D Casson nanofluid under the effect of Arrhenius activation energy and heat radiation. Kalaivanan *et al.* [7] (2015) used the confluent hypergeometric function to investigate the aligned magnetic field ascendancy on slip flow of Casson fluid past elongating sheet, and it was discovered that velocity distributions decreased as slip and Casson parameters increased, while temperature film increased as slip and Casson parameters increased. Jain and Parmar [8] (2017) investigate the entropy production of unsteady radiative Casson fluid flow through a porous material over a permeable stretched surface with an angled magnetic field. Devi *et al.* [9] (2021) used the Runge-Kutta technique to study the influence of an aligned magnetic field and an angled outer velocity on Casson fluid flow over a stretched sheet with a heat source. The results showed that when the outer velocity parameter is less than one, velocity decreases as the Casson fluid parameter, magnetic parameter, and aligned angle of magnetic field increase, whereas velocity increases when the outer velocity parameter is greater than one due to the formation of an inverted boundary layer for velocity profile in the second case. Seddeek [10] (2007) investigated heat and mass transfer in a viscoelastic fluid flow through a porous medium with a heat source or sink on a stretched sheet in the presence of a magnetic field.

Many engineering processes, including nuclear waste disposal, petroleum reservoirs, chemical catalytic processes and reactors, and many more, make use of double-diffusive fluid flow In a moving fluid, the phenomena of heat and mass transport processes occur concurrently; the energy fluxes created by the action of the composition gradient and temperature alongside the driving force are complex. The Soret or thermal-diffusion effect is the development of mass fluxes caused by a temperature gradient, whereas the Dufour or diffusion-thermo contribution is the development of energy fluxes induced by a composition gradient. Most literary scholars dismiss these effects since they are of a smaller magnitude

than the influence anticipated by Fick's law. Bilal *et al.* [11] (2016) investigated dissipative slip motion past a spinning cone using chemical reaction and Dufour-Soret processes. Jain and Choudhary [12] (2017) investigate the impact of Soret and Dufour on MHD fluid flow caused by moving permeable cylinders with radiation. In addition, Tai and Char [13] (2010) explore the Soret and Dufour effects on non-Newtonian fluid free convection flow down a vertical plate immersed in a porous medium with heat radiation. Non-Newtonian fluid flow, which includes both heat and mass transport phenomena, has recently sparked a lot of attention owing to its engineering applications. The bulk of non-Newtonian fluid rheological equations are quite complex and must be numerically solved. The Casson fluid motion is the most common type of non-Newtonian fluid motion. Jellies, jams, soups (food), blood, salvia (biological fluids), toothpaste, and other similar fluids are all examples. This fluid is used in polymer industries, heat exchangers, food processing, electronic cooling systems, and a number of other applications. Because of the numerous uses of non-Newtonian fluids, Fagbade *et al.* [14] (2018) successfully asserted the flowing nature of viscoelastic fluid past an accelerating penetrable surface by researching MHD natural convection. Mondal *et al.* [15] (2018) employed Soret-Dufour and thermophoresis to investigate MHD mixed convection mass transfer in an inclined plate. In addition to this effect, Ahmed *et al.* [16] (2020) elucidates the influence of Soret-Dufour mechanism, which accounts for buoyant force and viscous dissipation. Raza *et al.* [17] (2019) studied the quantitative flow of nanofluid MHD across a stretchy nonlinear porous surface. Using numerical analysis, Shafiq *et al.* [18] (2020) studied the sensitivity of the hyperbolic tangent of nanofluid bioconvective flow in a stretchy media. Hamid *et al.* [19] (2019) looked into the stability analysis and dual solutions of Casson fluid heat diffusion across an elastic surface. The free convective transient flow of a non-Newtonian fluid through a porous media is established in the work of Mabood *et al.* [20] (2020).

Previous studies did not look into the effects of an angled magnetic field on the flow of Casson nanofluids in the presence of Soret-Dufour and thermal radiation. The present research is focused on the Dynamics of Inclined Magnetic Fields, Brownian motion, and thermophoresis on the flow of electrically conducting and chemically reacting Casson nanofluids. This type of quandary, as far as we know, has never been addressed in the literature. SCM is used to solve the flow equations in this article. Graphs and tabular data are used to display numerical findings. The present study is useful in the manufacture of food and chemical engineering operations.

2. Mathematical Modeling

In this work, the dynamics of a two-dimensional model of an electrically conducting, incompressible, and viscous Casson nanofluid were investigated. The plate's surface temperature and concentration are considered to be where, and are temperatures and concentrations far from the boundary, and are wall tem-

peratures and concentrations (see Figure 1). The fluid's motion is assumed to be aided by an inclined magnetic field. The viscosity and thermal conductivity are assumed to be constant. We assumed that the magnetic Reynolds number is modest, thus we ignored induced magnetic. Thermal radiation and viscous dissipation are considered significant, allowing the fluid's thermal state to be rigorously investigated. Furthermore, a chemical process is thought to be occurring within the boundary layer. The flow constitutive equations for Casson are explained below using Fredrickson [21] (1964) and the definition of viscosity given by Idowu and Falodun [22] (2020) as the flow constitutive equations:

$$\begin{aligned} \tau_{ij} &= \left(\mu_b(T) + \frac{P_y}{\sqrt{2\pi}} \right) 2e_{ij} \quad \text{when } \pi > \pi_c \\ \tau_{ij} &= \left(\mu_b(T) + \frac{P_y}{\sqrt{2\pi_c}} \right) 2e_{ij} \quad \text{when } \pi < \pi_c \end{aligned} \tag{1}$$

where the fluid yield stress is P_y and mathematically written as:

$$P_y = \frac{\mu_b(T)\sqrt{2\pi}}{\beta} \tag{2}$$

μ_b defines plastic dynamic viscosity, $\pi = e_{ij}e_{ij}$ defines component product of deformation rate with itself and e_{ij} defines deformation rate and π_c defines critical value according to the model of Casson fluid. The Casson liquid motion where $\pi > \pi_c$, can be defined as:

$$\mu_0 = \mu_b(T) + \frac{P_y}{\sqrt{2\pi}} \tag{3}$$

when (2) is converted into (3), the kinematic viscosity becomes susceptible to

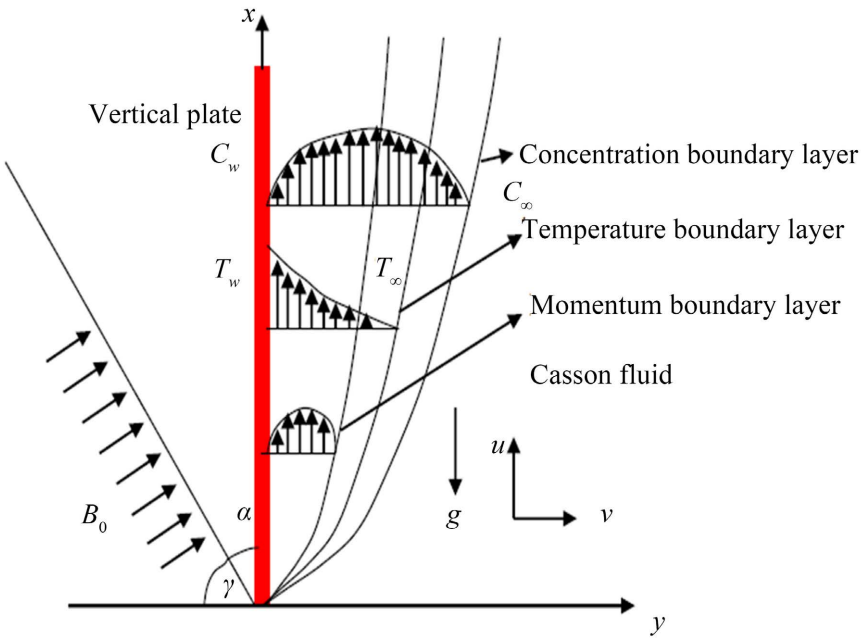

Figure 1. Graphic representation of the flow.

plastic dynamic viscosity μ_b, the density is ρ and the Casson term β resulted to:

$$\mu_0 = \frac{\mu_b(T)}{\rho}\left(1+\frac{1}{\beta}\right) \tag{4}$$

The Boussinesq approximation is considered to be valid such that the boundary layer approximation is explored. Hence, the following governing equations are derived based on the assumptions above:

$$\frac{\partial u}{\partial x}+\frac{\partial v}{\partial y}=0 \tag{5}$$

$$\begin{aligned} u\frac{\partial u}{\partial x}+v\frac{\partial u}{\partial y} &= \nu\left(1+\frac{1}{\beta}\right)\frac{\partial^2 u}{\partial y^2}-\frac{\sigma B_0^2}{\rho}\sin^2(\gamma)u+g\beta_t(T-T_\infty)\cos(\alpha) \\ &+ g\beta_c(C-C_\infty)\cos(\alpha)-\frac{\nu u}{K^*} \end{aligned} \tag{6}$$

$$\begin{aligned} u\frac{\partial T}{\partial x}+v\frac{\partial T}{\partial y} &= \alpha\frac{\partial^2 T}{\partial y^2}-\frac{1}{\rho c_p}\frac{\partial q_r}{\partial y}+\frac{\nu}{c_p}\left(1+\frac{1}{\beta}\right)\left(\frac{\partial u}{\partial y}\right)^2+\frac{\sigma B_0^2}{c_p\rho}\sin^2(\gamma)u^2 \\ &+\frac{Dk_T}{c_s c_p}\frac{\partial^2 C}{\partial y^2}+\tau\left[D_B\left(\frac{\partial C}{\partial y}\right)\left(\frac{\partial T}{\partial y}\right)+\frac{D_T}{T_\infty}\left(\frac{\partial T}{\partial y}\right)^2\right]+\frac{Q_0}{\rho C_p}(T-T_\infty) \end{aligned} \tag{7}$$

$$u\frac{\partial C}{\partial x}+v\frac{\partial C}{\partial y}=D_B\frac{\partial^2 C}{\partial y^2}+\frac{D_T}{T_\infty}\frac{\partial^2 T}{\partial y^2}-k_l(C-C_\infty)+\frac{Dk_T}{T_m}\frac{\partial^2 T}{\partial y^2} \tag{8}$$

Subject to the boundary constraints:

$$u=Bx,\ v=-\nu(x),\ T=T_w,\ C=C_w,\ \text{at } y=0 \tag{14}$$

$$u\to 0,\ T\to T_\infty,\ C\to C_\infty,\ \text{as } y\to\infty \tag{15}$$

u and v represents the relations $u=\frac{\partial\psi}{\partial y}$ and $v=-\frac{\partial\psi}{\partial x}$. In the definition of u and v, $\psi(x,y)$ is the free stream that always fulfills the continuity equation. The following are the definitions of similarity variables:

$$\eta=\left(\frac{B}{\nu}\right)^{\frac{1}{2}}y,\ \psi=(\nu B)^{\frac{1}{2}}xf(\eta),\ \theta(\eta)=\frac{T-T_\infty}{T_w-T_\infty},\ \phi(\eta)=\frac{C-C_\infty}{C_w-C_\infty} \tag{16}$$

Using Equation (16) on Equations (10)-(13) subject to (14) and (15) to obtain:

$$\begin{aligned} &\left(1+\frac{1}{\beta}\right)f'''+ff''+\left(1+\frac{1}{\beta}\right)f'f'''-(f')^2-M\sin^2(\gamma)f' \\ &+Gr\theta\cos(\alpha)+Gm\phi\cos(\alpha)-\frac{1}{P_0}f'=0 \end{aligned} \tag{17}$$

$$\begin{aligned} &\left(\frac{1+Nr}{Pr}\right)\theta''+Ec\left(1+\frac{1}{\beta}\right)(f'')^2+f\theta'+MEc\sin^2(\gamma)(f')^2 \\ &+Du\phi''+Nb\phi'\theta'+Nt(\theta')^2+Q\theta=0 \end{aligned} \tag{18}$$

$$\phi''+ScSo\theta''-ScCr\phi+Scf\phi'+\frac{ScNt}{LnNb}\theta''=0 \tag{19}$$

Subject to:

$$f' = 1,\ f = f_w,\ \theta = 1,\ \phi = 1,\ \text{at } \eta = 0 \tag{20}$$

$$f' \to 0,\ \theta \to 0,\ \phi \to 0\ \text{ as } \eta \to \infty \tag{21}$$

The control parameters are defined as follows:

$$M = \frac{\sigma B_0^2}{a\rho},\ Pr = \frac{\nu}{\alpha},\ Nr = \frac{16\sigma_s T^3}{3kk_e},\ Ec = \frac{(ax)^2}{c_p(T_w - T_\infty)},$$

$$Du = \frac{DK_T(C_w - C_\infty)}{c_s c_p \nu(T_w - T_\infty)},\ Sc = \frac{\nu}{D_B},\ So = \frac{D_T(T_w - T_\infty)}{T_\infty \nu(C_w - C_\infty)},\ Cr = \frac{k_l}{a},$$

$$Nb = \frac{\tau D_B(C_w - C_\infty)}{\nu},\ Nt = \frac{\tau D_T(T_w - T_\infty)}{T_\infty \nu},\ Q = \frac{Q_0}{\rho c_p b},\ Ln = \frac{\nu}{D_B}$$

Are the chemical reaction parameter, Thermophoresis parameter, Magnetic *M*, parameter, Prandtl number *Pr*, thermal radiation parameter *Nr*, Eckert number *Ec*, Dufour number *Du*, Schmidt number *Sc*, Brownian motion parameter *Nb*, heat generation parameter *Q*, Lewis number *Ln*, and Soret number *So*.

3. Method of Approach

The spectra Chebyshev collocation scheme is engaged for the numerical computation of the boundary value nonlinear derivative system of Equations (17)-(19). The following functions $f(\eta) = \sum_{i=0}^{N} a_i T_i(\eta)$, $\theta(\xi) = \sum_{i=0}^{N} b_i T_i(\eta)$, $\phi(\eta) = \sum_{i=0}^{N} c_i T_i(\eta)$ and are defined and approximated by the sum of the basic functions $T_n(\eta)$. The basis functions are chosen as the Chebyshev polynomials $T_n(\eta) = \cos\left(N\cos^{-1}\eta\right), -1 \le \eta \le 1$, were a_n, b_n and c_n are unidentified coefficients to be gotten. The flow range is $[0,\infty]$, but changed to $[-1,1]$ satisfying the defined basis polynomials, with $\eta = \frac{2\xi}{\xi_\infty} - 1$ where the far stream is taken as ξ_∞. Now, to have residual reduced to zero, substitute the values $f(\eta), \theta(\eta)$ and $\phi(\eta)$ into Equations (17)-(19), where the coefficient a_i, b_i, c_i and are picked to minimize the residues in the domain range. The collocation scheme is adopted in the form described by Khater *et al.* [23] (2000):

$$\eta_i = \cos\left(\frac{i\pi}{Z}\right),\ i = 0,1,2,3,\cdots,Z \tag{22}$$

This produces $3i+3$ an algebraic system of equations with $3i+3$ been the anonymous coefficients in terms of a_i, b_i and c_i. An iterative Newton's technique is used $i = 30$. Also, the BVP algorithm is established in Mathematical software to generate computational results.

4. Results and Discussion

This paper examines a numerical simulation of dimensionless velocity, concentration, and temperature for the flow model. The Chebyshev collocation method

is utilized in this paper to solve the transformed Equations (17)-(19) subject to (20) and (21). (21). The thermal Grashof number, magnetic parameter, Casson parameter, Eckert number, Brownian motion parameter, and so on all vary. We used = 3.0, $Gr = Gm = 0.5$, $M = 1.0$, $Ec = 0.01$, $Du = 2.0$, $Nb = Nt = 0.7$, $Cr = 0.2$, and $So = 1.0$ as the default settings for presenting all figures and creating tables. To establish the validity of the current work, we first solved a specific example of our model and then compared it to the prior results of Gopal and Kishan [24] (2019). Our findings in **Table 1** were entirely consistent with theirs.

The effect of the Casson parameter on the velocity figure is seen in **Figure 2**. Raising the Casson parameter reduces fluid velocity when the viscosity and thermal conductivity are both constant. This is due to flow resistance caused by the fluid's plastic dynamic viscosity. As seen in **Figure 2**, raising the Casson parameter

Table 1. Comparison of the present results with that of Gopal and Kishan [24] (2019) when $So = Du = 0$.

β	Gr	Gm	Ha	Ec	Du	Cr	So	Cf	Nu	Sh
0.2								0.2085	0.6110	0.8123
0.4								0.4219	0.6110	0.8123
0.6								0.9312	0.6110	0.8123
	0.5							0.7499	0.3581	0.3899
	1.0							1.4328	0.3581	0.3899
	2.0							2.1156	0.3581	0.3899
		0.5						0.2285	0.6935	0.8633
		1.0						0.5296	0.6935	0.8633
		2.0						0.8306	0.6935	0.8633
			0.0					1.7682	0.8119	0.3513
			0.5					1.4328	0.8119	0.3513
			1.0					0.6530	0.8119	0.3513
				0.1				1.6306	0.4365	0.3899
				0.2				1.8285	0.7793	0.3899
				0.3				2.0264	0.8778	0.3899
					1.0			1.4328	0.6935	0.3106
					2.0			1.5532	0.5559	0.3106
					3.0			1.6736	0.4183	0.3106
						1.0		1.5069	0.6935	0.7655
						2.0		1.4328	0.6935	0.8633
						3.0		1.2533	0.6935	1.0904
							2.0	1.6885	0.8119	0.5353
							4.0	1.9443	0.8119	0.2074
							6.0	2.2000	0.8119	−0.1205

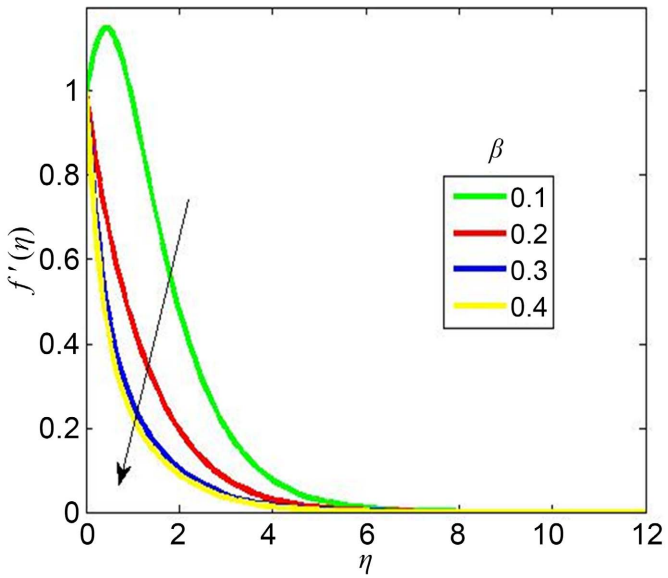

Figure 2. Consequence of Casson parameter on the velocity profile.

increases the fluid velocity figure as well as the total hydrodynamic boundary layer. Physically, the presence of an angled magnetic field, as well as plastic dynamic viscosity, causes the electrically conducting Casson fluid investigated in this work to move slowly. Figure 3 elucidates the impact of the thermal Grashof number (*Gr*) on velocity. Because it has sped up fluid particle mobility, *Gr* serves as a buoyant force on the fluid flow. *Gr* is a dimensionless quantity ratio of buoyancy to viscous force defined by the fluid inside the layer. When the thermo-physical parameters stay constant, increasing the values of *Gr* causes an enhancement in the velocity figure and total hydrodynamic boundary layer thickness. In practice, increased thermal buoyancy indicates a laminar flow. Figure 4 depicts the impact of the mass Grashof number (*Gm*) on velocity. The fluid motion increases as the value of *Gm* rises. The fluid velocity reaches its maximum as the species' buoyancy force grows. The velocity has reached its peak within the plate zone and is decreasing as it approaches the free stream. Figure 5 depicts the effect of the Eckert number (*Ec*) on velocity and temperature graphs. The dimensionless number in heat and mass transfer represents the viscous dissipation factor that is applied to the energy equation. *Ec* is a velocity-dependent function that defines the relationships between flow kinetic energy and enthalpy. Work done by Ec physically transfers kinetic energy to internal energy. Figure 5 depicts the fluid temperature distribution when the viscous dissipative heat is higher. Figure 6 illustrates the influence of a chemical reactive parameter (*Cr*) on the profiles of velocity and concentration respectively. The velocity and concentration graphs degrade as *Cr* concentrations rise. A chemical reaction takes place on the fluid particles and the magnetic field angled toward the plate. A decline in fluid velocity and concentration distributions implies a hazardous chemical reaction taking place within the hydrodynamic and specie boundary layers. Figure 7 elucidate the effect of the Hartmann number (*Ha*) on a fluid velocity

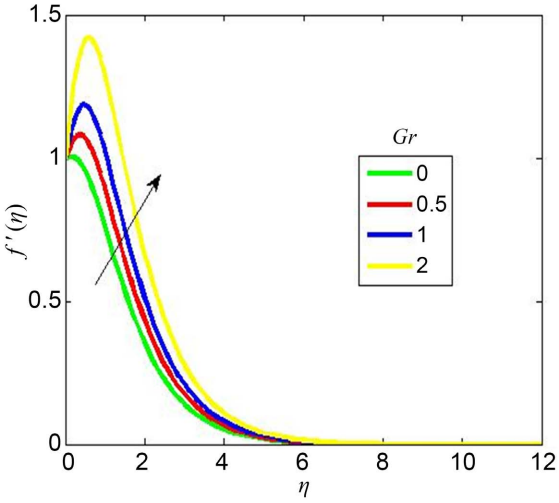

Figure 3. Consequence of thermal Grashof number on the velocity profile.

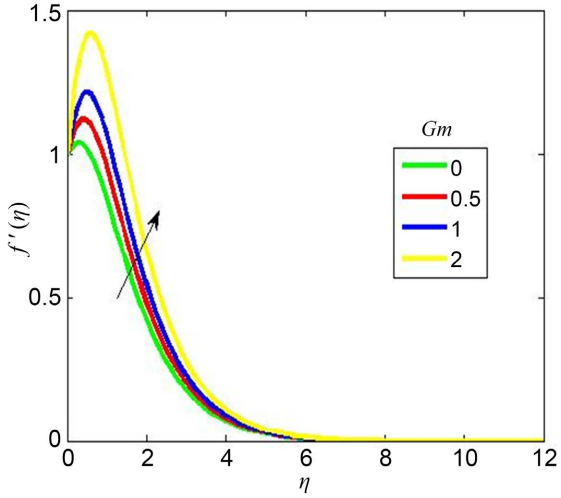

Figure 4. Consequence of mass Grashof number on the velocity profile.

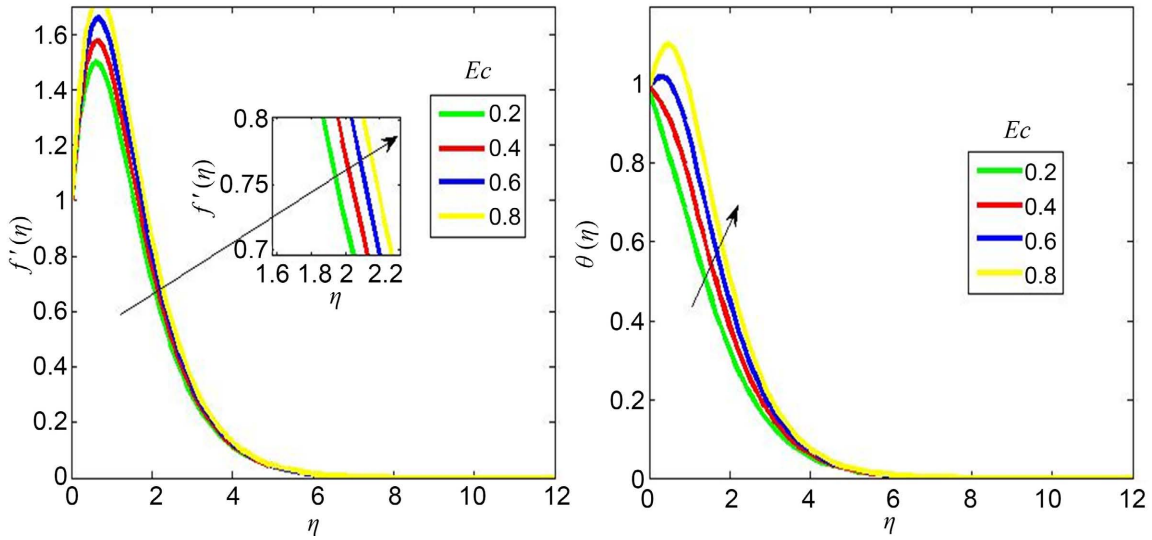

Figure 5. Consequence of Eckert number on the velocity and temperature profiles.

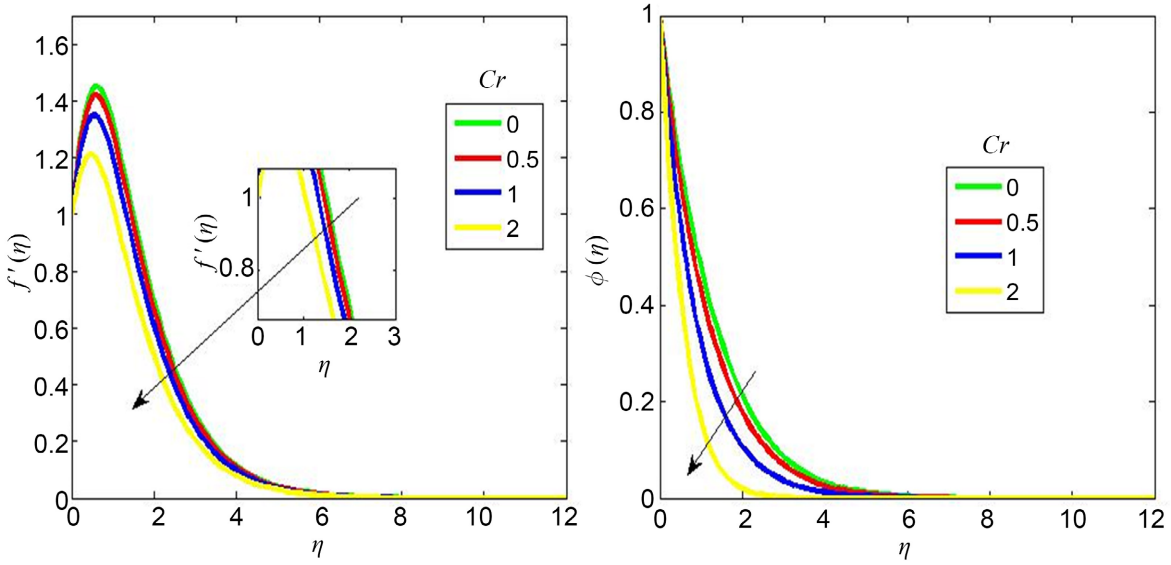

Figure 6. Consequence of chemical reaction parameter on the velocity and concentration profiles.

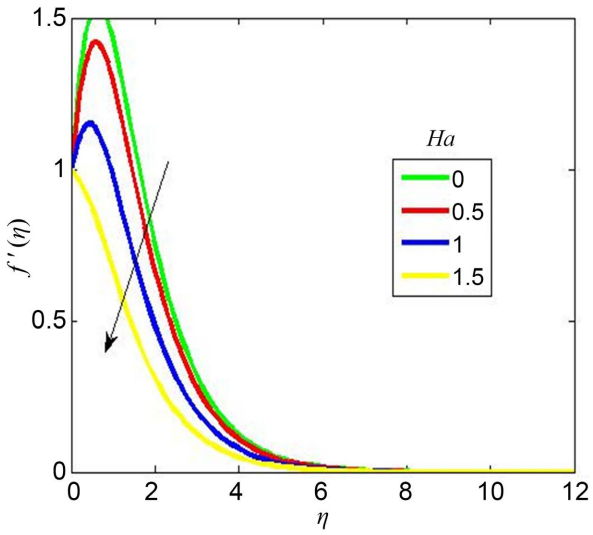

Figure 7. Consequence of Hartmann number on the velocity profile.

curve. When the Hartmann number (*Ha*) is raised, the fluid velocity distribution shrinks. The Hartmann number is a gadget that has a significant influence on an electrically conducting fluid. In our model, an increase in the Hartmann number results in a significant drop in the velocity distribution and overall thickness of the hydrodynamic boundary layer for the case of an inclined magnetic field. This is because when the Hartmann number grows, so does the Lorentz force, which takes charge of lowering the velocity of electrically conducting fluids like the Casson fluid under consideration in this study. In Figure 8, the influence of the Soret parameter (*So*) on velocity and species distributions is illustrated. The value of *So* rises, raising both the velocity and concentration distributions. In the heat and mass transfer scenario, the Soret parameter (*So*) varies with temperature, but it is always included in the species equation. A larger Soret parameter

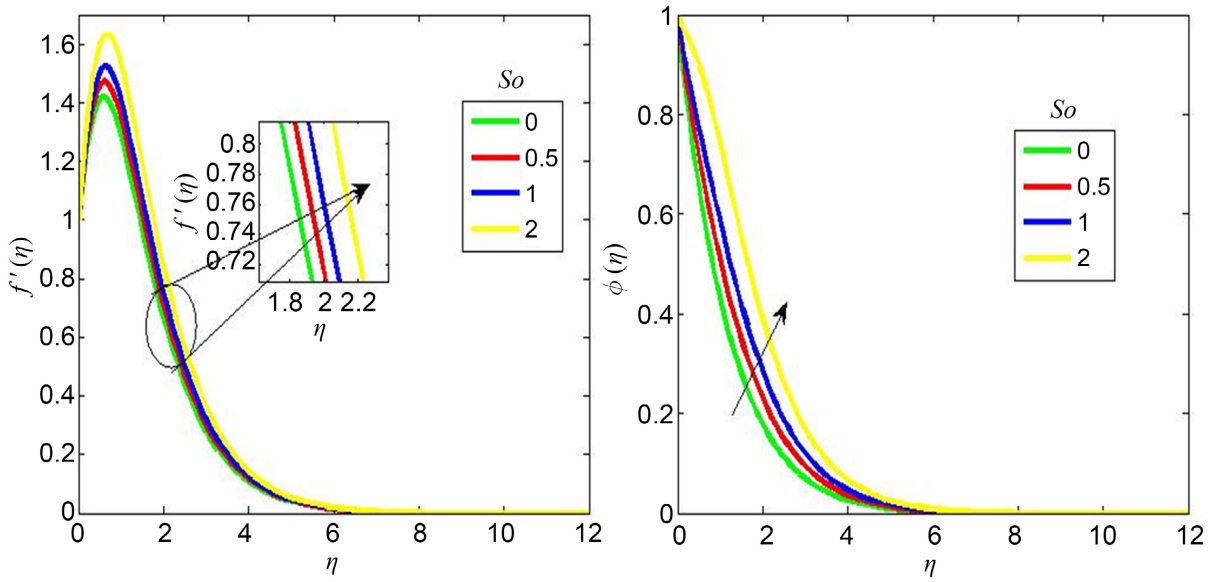

Figure 8. Consequence of Soret parameter on the velocity and concentration profiles.

leads to exceptionally rapid migration of Casson nanofluid particles from the hot to the cold zone in the case of constant thermo-physical parameters investigated in this work. This kind of contribution is essential in isotope separation's chemical engineering application. Figure 9 and Figure 10 show how the Dufour parameter influences the velocity and temperature distributions. Although it is usually included in the energy equation in the scenario of heat and mass transfer, it is a function of concentration in the physical phenomena of Dufour term. A greater Dufour parameter value drove the fluid particles into an environment where heat energy became critical. Heat energy improves the thermal condition of the fluid by increasing temperature distributions in the situation of constant thermo-physical parameters and an inclined magnetic field. Figure 10 depicts the effect of the Brownian motion parameter on velocity and temperature curves. The velocity and temperature profiles improve as the Brownian motion parameter values are increased. Brownian motion increases the speed of fluids within the boundary layer. A random collision of fluid particles speeds up heat transfer within the boundary layer. As a result, the temperature distribution skews more. Figure 11 depicts the influence of thermal radiation on velocity and temperature distributions. Thermal radiation contributes to the thermal state of the fluid layer physically. Raising the thermal radiation levels is now equal to increasing the fluid's thermal state. As a result, it enhances the amounts of thermal radiation upshots the fluid's speed and temperature distributions throughout the domain. Figure 12 shows the influence of the Prandtl number on velocity and temperature distributions. A higher Prandtl number indicates more viscosity, which decreases velocities and, as a result, skin friction. Physically, a rise in the Prandtl number correlates with a reduction in fluid temperature and thermal boundary layer thickness. As a consequence, the fluid becomes quite welcoming. Figure 13 depicts the influence of the Schmidt number on fluid flow and concentration

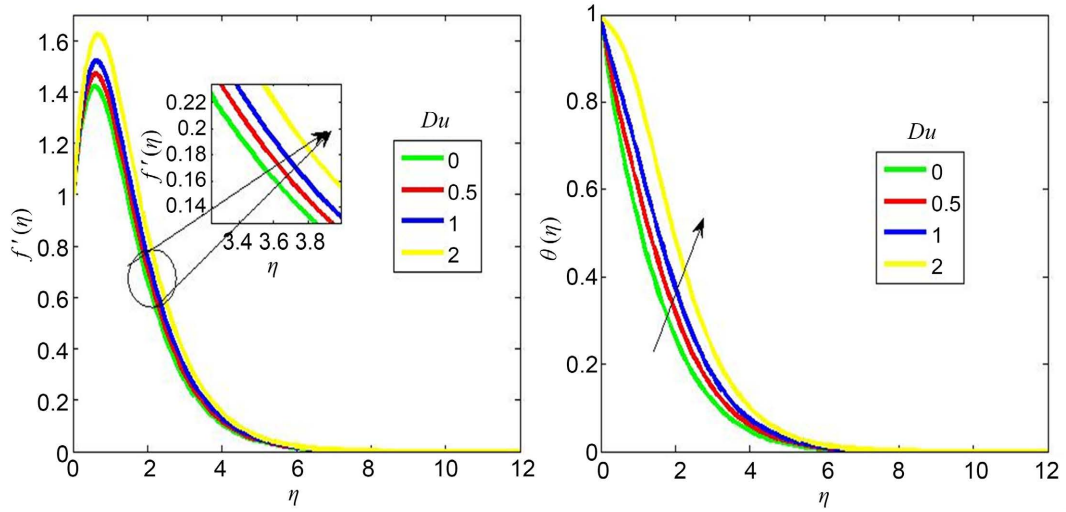

Figure 9. Consequence of Dufour parameter on the velocity and temperature profiles.

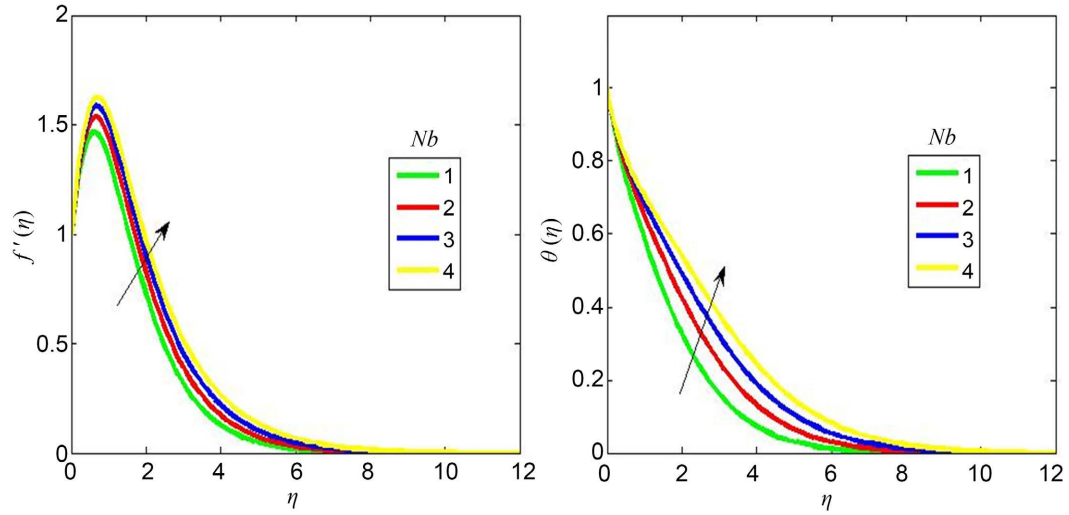

Figure 10. Consequence of Brownian motion on the velocity and temperature profiles.

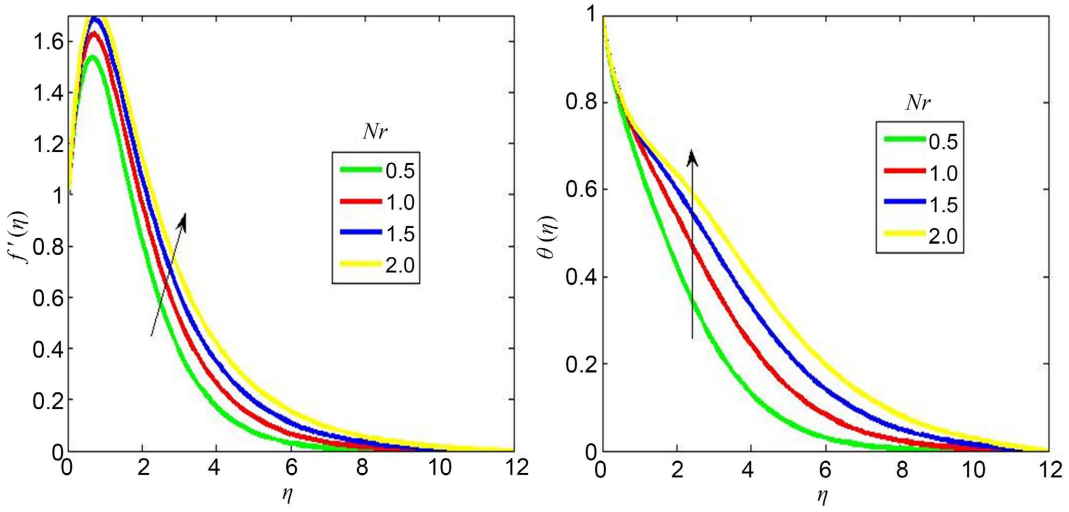

Figure 11. Consequence of thermal radiation on the velocity and temperature profiles.

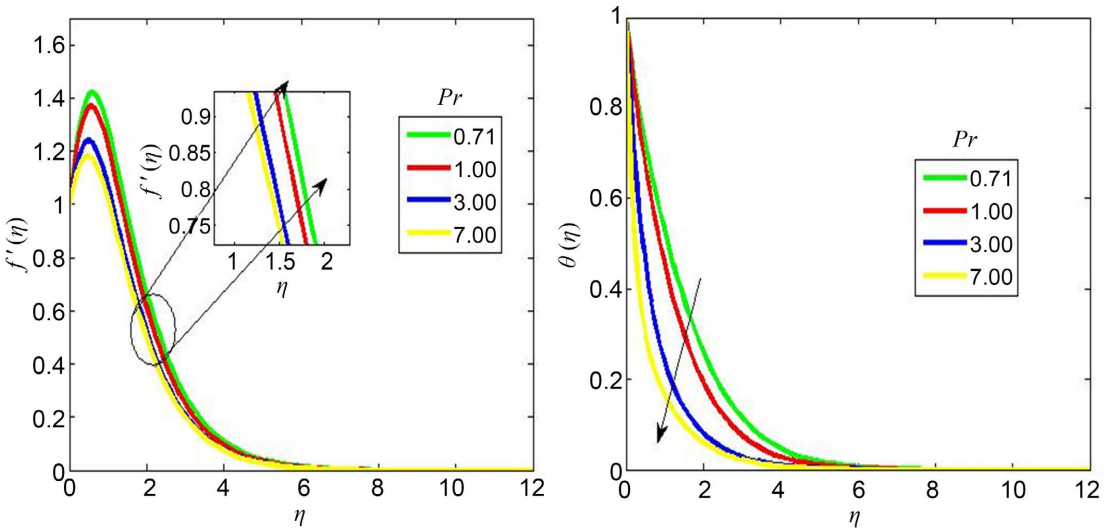

Figure 12. Consequence of Prandtl number on the velocity and temperature profiles.

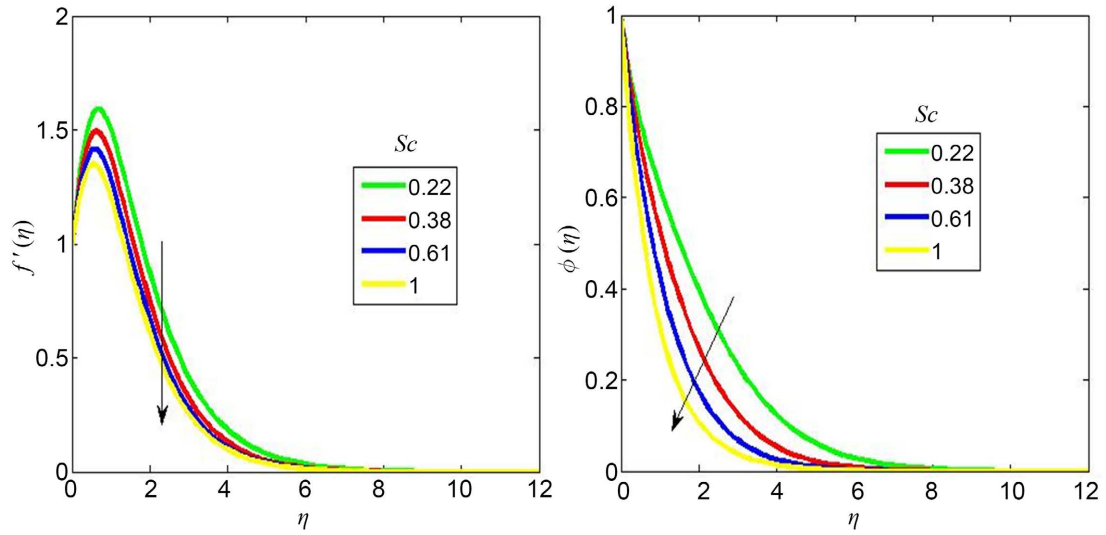

Figure 13. Consequence of Schmidt number on the velocity and concentration profiles.

patterns. Figure 13 shows how raising the concentration profile degenerates. It is the inverse percentage of the Brownian diffusion coefficient. As the moment rises, Brownian diffusion slows; causing the concentration to fall and alike result was established through Uddin *et al.* [25] (2019). Raising resulted in the same rate of spontaneous species spread, according to our numerical simulation. It's important to note that when there's a lot of species dispersion, the momentum diffusivity increases. The absence of species concentration is referred to as a "setting". Rising presently reduces fluid concentration and reduces its visibility.

Table 2 depicts the effect of physical characteristics such as engineering factors of significance such as local skin friction, Nusselt and Sherwood number. Increased Casson parameter value increases local skin friction but has little change on Nusselt and Sherwood values. It has been discovered that increasing the thermal Grashof number and mass Grashof number raises the hydrodynamic

Table 2. Contributions of β, *Gr*, *Gm*, *Ha*, *Du*, *Cr*, and *So* on the local skin friction (*Cf*), Nusselt number and Sherwood number.

			Present study			Gopal and Kishan [24] (2019)		
M	*Pr*	β	$\left(1+\frac{1}{\beta}\right)C_f(0)$	*Nu*	*Sh*	$\left(1+\frac{1}{\beta}\right)C_f(0)$	*Nu*	*Sh*
1			0.217582	0.432130	0.451896	0.217574	0.432128	0.451893
2			0.128460	0.43677	0.440688	0.128458	0.436076	0.0440687
3			0.049672	0.438545	0.432230	0.049668	0.438544	0.432229
	0.5		0.296826	0.506368	0.364582	0.296824	0.506367	0.364580
	1.0		0.381842	0.735880	0.045983	0.381841	0.735878	0.045981
	1.5		0.432253	0.897216	0.020607	0.432251	0.897214	0.020605
		1	0.200100	0.3603347	0.576828	0.200109	0.360345	0.576826
		2	0.210308	0.362645	0.578047	0.201306	0.362643	0.578045
		3	0.202275	0.363484	0578049	0.202273	0.363482	0.578045

boundary layer, therefore increasing local skin friction. A species' buoyant force is calculated using the thermal Grashof number. As the Hartmann number grows, so does the local skin friction along with the hydrodynamic boundary layer. A greater Eckert number improves local skin friction as well as the Nusselt number. As a result of excessive heat dissipation, the Eckert number generates kinetic energy, which is transformed to heat energy. A greater value of the chemical reaction parameter was shown to decrease the rate of mass transfer, whereas a higher value of the Soret and Dufour parameters was discovered to enhance the rate of mass transport. Increase the rate of heat and mass transfer.

5. Conclusions

The spectral collocation approach was used to address the scenario of the dynamics of an angled magnetic field on the flow of Casson nanofluids under the effect of the Soret-Dufour mechanism. The results of the numerical calculations were graphed, while the calculations of engineering quantities of importance were discussed through tables. This study's major results are as follows:

1) The inclined magnetic parameter is shown to have a considerable effect on fluid flow within the boundary layer by slowing down the fluid velocity distribution.

2) The Casson fluid's plastic dynamic viscosity is detected to decelerate the fluid hydrodynamic boundary layer for a higher Casson parameter.

3) A greater value of the chemical reaction parameter is seen to reduce the fluid motion and concentration distributions.

4) The thermal Grashof number is seen to operate as a buoyancy force by significantly increasing the fluid motion.

5) The combined impacts of the Soret and Dufour processes are evident in the temperature and concentration distributions. An additional value of the Soret

parameter influences fluid concentration by raising the distribution, whereas the Dufour parameter increases fluid temperature by elevating the profile.

6) The temperature boundary film tends to decline with an augmentation in the Prandtl number due to strong ambient heat diffusion.

As a result of better heat conduction and chemical species propagation, the findings in this work are critical to thermal engineering science and valuable in the growth of nanotechnology.

It will also aid in the enhancement of hydromagnetic lubricant due to the strong thermal conduction of Casson nanofluid. As a result, the research may be expanded to include flow in a concentric cylinder.

Conflicts of Interest

The authors declare no conflicts of interest regarding the publication of this paper.

References

[1] Alao, F.I., Fagbade, A.I. and Falodun, B.O. (2016) Effects of Thermal Radiation, Soret and Dufour on an Unsteady Heat and Mass Transfer Flow of a Chemically Reacting Fluid Past a Semi-Infinite Vertical Plate with Viscous Dissipation. *Journal of the Nigerian Mathematical Society*, **35**, 142-158. https://doi.org/10.1016/j.jnnms.2016.01.002

[2] Parvin, S., Isa, S.S.P.M., Arifin, N. and Ali, F. (2021) The Inclined Factors of Magnetic Field and Shrinking Sheet in Casson Fluid Flow, Heat and Mass Transfer. *Symmetry*, **13**, Article No. 373. https://doi.org/10.3390/sym13030373

[3] Saravana R., Sailaja, M. and Hemadri Reddy, R. (2019) Effect of Aligned Magnetic Field on Casson Fluid Flow over a Stretched Surface of Non-Uniform Thickness. *Nonlinear Engineering*, **8**, 283-292. https://doi.org/10.1515/nleng-2017-0173

[4] Hashim, H., Sarif, N., Salleh, M.Z. and Mohamed, M.K.A. (2020) Aligned Magnetic Field on Williamson Fluid over a Stretching Sheet with Newtonian Heating. *Journal of Physics*: *Conference Series*, **1529**, Article ID: 052085. https://doi.org/10.1088/1742-6596/1529/5/052085

[5] Yusuf, T.A and Mabood, F. (2020) Slip Effects and Entropy Generation on Inclined MHD Flow of Williamson Fluid through a Permeable Wall with Chemical Reaction via DTM. *Mathematical Modelling of Engineering Problems*, **7**, 1-9. https://doi.org/10.18280/mmep.070101

[6] Jawad, M., Saeed, A., Taza, G. and Bariq, A. (2021) MHD Darcy-Forchheimer Flow of Casson Nanofluid Due to a Rotating Disk with Thermal Radiation and Arrhenius Activation Energy. *Journal of Physics Communications*, **5**, Article ID: 025008. https://doi.org/10.1088/2399-6528/abe4e0

[7] Kalaivanan, R., Renuka, P., Vishnu Ganesh, N., Abdul Hakeem, A.K., Ganga, B. and Saranya, S. (2015) Effects of Aligned Magnetic Field on Slip Flow of Casson Fluid over a Stretching Sheet. *Procedia Engineering*, **127**, 531-538. https://doi.org/10.1016/j.proeng.2015.11.341

[8] Jain, S. and Parmar, A. (2017) Entropy Generation of Unsteady Radiative Casson Fluid Flow through Porous Medium over a Permeable Stretching Surface with an Inclined Magnetic Field. *Frontiers in Heat and Mass Transfer* (*FHMT*), **9**, Article No. 40. https://doi.org/10.5098/hmt.9.40

[9] Devi, R., Poply, V. and Mala, M. (2021) Effect of Aligned Magnetic Field and Inclined Outer Velocity in Casson Fluid Flow over a Stretching Sheet with Heat Source. *Journal of Thermal Engineering*, **7**, 823-844. https://doi.org/10.18186/thermal.930347

[10] Seddeek, M.A. (2007) Heat and Mass Transfer on a Stretching Sheet with a Magnetic Field in a Viscoelastic Fluid Flow through a Porous Medium with Heat Source or Sink. *Computational Materials Science*, **38**, 781-787. https://doi.org/10.1016/j.commatsci.2006.05.015

[11] Bilal, S., Rehman, K.U., Jamil, H., Malik, M.Y. and Salahuddin, T. (2016) Dissipative Slip Flow along with Heat and Mass Transfer over a Vertically Rotating Cone by Way of Chemical Reaction with Dufour and Soret Effects. *AIP Advances*, **6**, Article ID: 125125. https://doi.org/10.1063/1.4973307

[12] Jain, S., and Choudhary, R., (2017) Soret and Dufour Effects on MHD Fluid Flow Due to Moving Permeable Cylinder with Radiation. *Global and Stochastic Analysis*, **4**, 75-84.

[13] Tai, B.C. and Char, M.I. (2010) Soret and Dufour Effects on Free Convection Flow of a Non-Newtonian Fluid along a Vertical Plate Embedded in a Porous Medium with Thermal Radiation. *International Communications in Heat and Mass Transfer*, **37**, 480-483. https://doi.org/10.1016/j.icheatmasstransfer.2009.12.017

[14] Fagbade, A.I., Falodun, B.O. and Omowaye, A.J. (2018) MHD Natural Convection Flow of Viscoelastic Fluid over an Accelerating Permeable Surface with Thermal Radiation and Heat Source or Sink: Spectral Homotopy Analysis Approach. *Ain Shams Engineering Journal*, **9**, 1029-1041. https://doi.org/10.1016/j.asej.2016.04.021

[15] Hiranmoy, M., Pal, D., Chatterjee, S. and Sibanda, P. (2018) Thermophoresis and Soret Dufour on MHD Mixed Convection Mass Transfer over an Inclined Plate with Non-Uniform Heat Source/Sink and Chemical Reaction. *Ain Shams Engineering Journal*, **9**, 2111-2121. https://doi.org/10.1016/j.asej.2016.10.015

[16] Ahmed, L.O., Falodun, B.O. and Abdulwaheed, J. (2020) Mechanism of Soret-Dufour, Magnetohydrodynamics, Heat and Mass Transfer Flow with Buoyancy Force, and Viscous Dissipation Effects. *Heat Transfer*, **49**, 2831-2848. https://doi.org/10.1002/htj.21748

[17] Raza, J., Farooq, M., Fateh, M.O. and Mahanthesh, B. (2019) Multiple Slip Effects on MHD Non-Newtonian Nanofluid Flow over a Nonlinear Permeable Elongated Sheet Numerical and Statistical Analysis. *Multidiscipline Modelling in Materials and Structures*, **15**, 913-931. https://doi.org/10.1108/MMMS-11-2018-0190

[18] Shafiq, A., Sindhu, T.N. and Khalique, C.M. (2020) Numerical Investigation and Sensitivity Analysis on Bioconvective Tangent Hyperbolic Nanofluid Flow towards Stretching Surface by Response Surface Methodology. *Alexandria Engineering Journal*, **59**, 4533-4548. https://doi.org/10.1016/j.aej.2020.08.007

[19] Hamid, M., Usman, M., Khan, Z.H., Ahmad, R. and Wang, W. (2019) Dual Solutions and Stability Analysis of Flow and Heat Transfer of Casson Fluid over a Stretching Sheet. *Physics Letters A*, **383**, 2400-2408. https://doi.org/10.1016/j.physleta.2019.04.050

[20] Mabood, F., Yusuf, T.A. and Sarris, I.E. (2020) Entropy Generation and Irreversibility Analysis on Free Convective Unsteady MHD Casson Fluid Flow over a Stretching Sheet with Soret/Dufour in Porous Media. *Special Topics & Reviews in Porous Media: An International Journal*, **11**, 595-611. https://doi.org/10.1615/SpecialTopicsRevPorousMedia.2020033867

[21] Fredrickson, A.G. (1964) Principles and Applications of Rheology. Prentice-Hall, Englewood Cliffs, NJ.

[22] Idowu, A.S. and Falodun, B.O. (2020) Effects of Thermophoresis, Soret-Dufour on Heat and Mass Transfer Flow of Magnetohydrodynamics Non-Newtonian Nanofluid over an Inclined Plate. *Arab Journal of Basic and Applied Sciences*, **27**, 149-165. https://doi.org/10.1080/25765299.2020.1746017

[23] Khater, A.H., Shamardan, A.B., Callebaut, D.K. and Ibrahim, R.S. (2000) Chebyshev Spectral Collocation Methods for nonlinear Isothermal Magnetostatic Atmospheres. *Journal of Computational and Applied Mathematics*, **115**, 309-329. https://doi.org/10.1016/S0377-0427(99)00306-4

[24] Gopal, D. and Kishan, N. (2019) Brownian Motion and Thermophoresis Effects on Casson Nanofluid over a Chemically Reacting Stretching Sheet with Inclined Magnetic Field. *Applications and Applied Mathematics*: *An International Journal* (*AAM*), **14**, Article No. 9. https://digitalcommons.pvamu.edu/aam/vol14/iss4/9

[25] Uddin, N., Alim, A. and Rahman, M. (2019) MHD Effects on Mixed Convective Nanofluid Flow with Viscous Dissipation in Surrounding Porous Medium. *Journal of Applied Mathematics and Physics*, **7**, 968-982. https://doi.org/10.4236/jamp.2019.74065